Experiments in Atmospheric Predictability: Part I. Initialization

WILLIAM BLUMEN

Department of Astro-Geophysics, University of Colorado, Boulder 80309

(Manuscript received 27 May 1975, in revised form 30 September 1975)

ABSTRACT

Predictability experiments are carried out with a divergent barotropic model that describes the evolution of quasi-geostrophic planetary waves and high-frequency gravity-inertia waves. Error growth, relative to a model-determined control state, is initiated by an initialization procedure that is not compatible with the model equations. An analysis of error growth due to improper representation of the physics incorporated in prediction models is also carried out with the present model. The error growth rate and the range of predictability determined from these experiments, based on a simple triad solution of the nonlinear forecast equation, compare very well with the results from experiments carried out with multi-level numerical models. The mechanism of predictability decay by nonlinear energy exchange is shown to differ from the corresponding mechanism discussed by Lorenz and Leith, which is based on a model of two-dimensional turbulence.

1. Introduction

The growth rate of initial errors in numerical weather prediction models has attracted widespread interest among meteorologists because this problem is intrinsically related to the inherent limit of predictability of the atmosphere. Numerical models used for operational and research purposes are quite complex, incorporating multi-layers and many parameterizations of physical processes. Consequently, it is very difficult to accurately diagnose prediction errors in order to distinguish between errors caused by numerical truncation, and imperfect initialization and parameterization procedures. Recent publications by Kasahara (1972) and Bengtsson (1975) provide overviews of recent investigations intended to isolate and evaluate the relative importance of each type of error. At the same time, these efforts are also directed to establishing methods for improving the accuracy of short-term forecasts and extending the limit of deterministic predictability.

Numerical experimentation has primarily provided information on the response of different models to various initial errors in terms of model parameters, such as horizontal and vertical grid spacing and physical parameterizations. Forecast improvement, based on this information, has thus far been minor. In part, the lack of good quality and quantity of meteorological observations affects forecast accuracy; in part, the problem lies with a certain lack of understanding of *why* models respond in a characteristic manner. Without this understanding, model improvements will be accomplished, if at all, by trial and error procedures. Though the atmosphere appears to be a highly complicated fluid system, this does not imply that significant reduction of forecast error variance can be attained only by increasingly sophisticated numerical and physical model refinements. For example, numerical experiments performed by Williamson and Kasahara (1971) show that theoretical deductions concerning eddy kinetic energy growth and the process of geostrophic adjustment, based on relatively simple atmospheric models, are verified reasonably well by the NCAR General Circulation Model (GCM). A recent theoretical analysis (Blumen 1975a) of root mean square (rms) forecast error growth, due to differences in propagation speed between forecast and control solutions of a barotropic model, also shows good agreement with NCAR GCM truncation error experiments performed by Williamson (1973). Thus it appears that future progress in the field of numerical weather prediction and circulation modeling will have to depend on a judicious mix of analytical and numerical studies.

In this and a companion paper (Part II) simple analytical predictability experiments are described. Attention is directed to predictability error growth, its causes, and possible means to control it by updating procedures. The present investigation differs from the previous study reported by the author (Blumen, 1975a, b) because here nonlinear interactions are incorporated in the model, introduced in Section 2. The method of initialization by the balance equation, which is responsible for error growth in the model, is described in Section 3. Model predictability associated with amplitude and phase errors is taken up, respectively, in Sections 4 and 5. Some interpretative remarks are presented in Section 6 and, in the Appendix, a nonlinear

solution of the model equation is developed. A description of the updating experiment and analyses of assimilation techniques appear in Part II.

2. Model

The development of the model used in the present study has been discussed in detail in previous publications (Blumen, 1972, 1975a). Hereafter Blumen (1975a) will be referred to as A. Briefly, a barotropic model, with depth-independent divergence in a bottom layer D_0 capped by an infinitely deep inert top layer, is employed. A two time-scale expansion is used to determine the zero-order system of equations that describe the relatively slow temporal evolution of the quasi-geostrophic field and the more rapid changes associated with the high-frequency gravity-inertia waves. This lowest-order system is coupled only through the initial conditions. The basic equations are the quasi-geostrophic forecast equation

$$\left(\frac{\partial}{\partial\tau}+U\frac{\partial}{\partial x}+V\frac{\partial}{\partial y}\right)\Omega_0=0, \tag{1}$$

and the wave equation, governing ageostrophic motion,

$$\left(\frac{\partial^2}{\partial T^2}+1-\lambda^2\Delta\right)\psi=0. \tag{2}$$

In (1) and (2) the slow time is $\tau=\mathrm{Ro}\,t$ and the fast time is $T=t$, where t denotes time, nondimensionalized by the Coriolis parameter $f_0=2\Omega\sin\phi_0$; $\mathrm{Ro}=U_0/f_0L\sim10^{-1}$ is the Rossby number defined for values of zonal wind U_0 and quarter-wavelength L typical of midlatitude synoptic-scale flow; and $\Delta=\partial^2/\partial x^2+\partial^2/\partial y^2$. The geostrophic potential vorticity is expressed by

$$\Omega_0=(\Delta-\lambda^{-2})\Psi+\beta y, \tag{3}$$

where $\beta=df/dy=$ constant, and λ is the nondimensional radius of deformation

$$\lambda=(g'D_0)^{\frac{1}{2}}f_0^{-1}L^{-1}, \tag{4}$$

which is expressed in terms of reduced gravity g'. The geostrophic streamfunction $\Psi=\Psi(x,y,\tau)$ evolves according to (1), the ageostrophic streamfunction $\psi=\psi(x,y,T,\tau)$ satisfies (2), and the complete zero-order solution is

$$\psi_0(x,y,T,\tau)=\Psi+\psi. \tag{5}$$

The geostrophic velocity components in (1) are determined from

$$U=-\partial\Psi/\partial y,\quad V=\partial\Psi/\partial x, \tag{6}$$

where (x,y) are the Cartesian coordinates, directed toward the east and north, respectively, and the flow domain is an unbounded beta-plane. The interested reader will find further details concerning the mathematical development and nondimensionalization in the references cited above.

3. Initialization

Three initial conditions are needed to determine the arbitrary constants arising in the solutions of (1) and (2). These are given, to zero-order, by specifying ψ_0, $\partial\psi/\partial T$ and $\partial^2\psi/\partial T^2$ at the initial time. As will be shown, these conditions are sufficient to determine the initial ageostrophic and geostrophic streamfields ψ and Ψ, which are displayed in (18) and (20).

Suppose that the quasi-geostrophic forecast equation (1) describes the evolution of the true state of the atmosphere. Then if the initial streamfield is accurately observed, such that $\psi_0=\Psi(x,y,0)$, $\partial\psi/\partial T=\partial^2\psi/\partial T^2=0$, Eq. (1) will provide a perfect forecast of $\Psi(x,y,\tau)$ at any future time with $\psi(x,y,T,\tau)\equiv0$. However, suppose the initial streamfield is incorrectly specified, differing in amplitude from the true value, for example, by an amount ϵ. As shown by Williamson and Dickinson (1972) and in A, a portion of the initial energy will be partitioned to gravity-inertia waves and the remainder to the geostrophic flow field. If both the atmospheric state and the forecast are governed by a *linearized version* of (1), then the rms forecast error will not exceed ϵ in magnitude. Moreover, it was demonstrated that periodic updating by the true pressure field could reduce the forecast error to zero.

In general, a forecast of $\Psi(x,y,\tau)$ from (1), using an incorrect initial value, will lead to an error growth until a level is reached that represents the difference between randomly chosen states. However, before this level is reached, the forecast has lost practical significance. Some typical rms error curves, determined from the NCAR GCM, are shown in Fig. 1, taken from

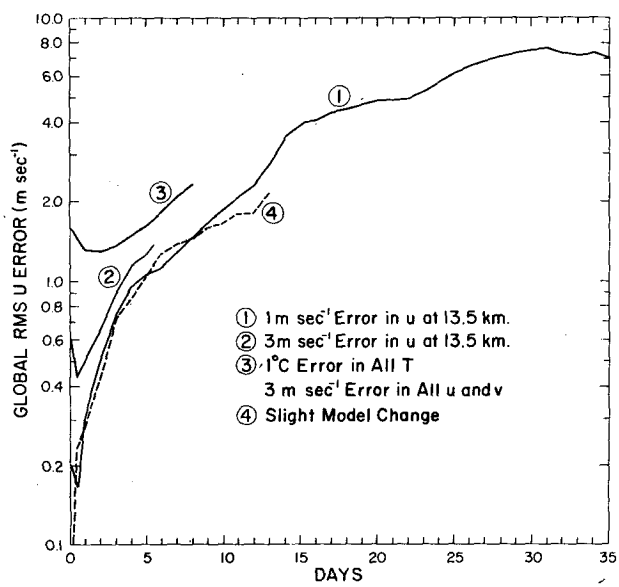

FIG. 1. Growth of rms error in zonal wind component from NCAR GCM experiments. The initial errors are given in the figures; the slight model change is discussed in Section 5 of the text.

Williamson and Kasahara (1971). Other numerical models show similar growth characteristics. This error growth is attributed to the nonlinear advective terms appearing in the model equations. Lorenz (1969) has shown, for example, that an initial error confined to the smallest scale of motion would spread to large scales, by nonlinear transfer, until the largest scale is affected by this error. The predictive value of the forecast model is first diminished, then lost. The maximum forecast error is attained in 2–3 weeks. A small error, initially confined to the largest scale of motion, shows a comparable range and level of predictability for all scales of motion. Lorenz interpreted these results to mean that *the range of predictability and the ultimate error level, representing the difference between randomly chosen states, is essentially independent of the initial error energy spectrum.* The results shown in Fig. 1 appear to be in agreement with this conclusion: the asymptotic error is essentially independent of the initial errors. Curves 2 and 3 in Fig. 1 were not extended to their asymptotic level, to save computer time. However, later experiments with the NCAR GCM, reported by Williamson (1973), do confirm the above conclusion.

The type of predictability experiments performed by Williamson and Kasahara, and others, may be characterized as "identical twin" experiments. A control run establishes the history of the "model atmosphere." If at some time a random error is introduced, to simulate an initial observation error in one or more meteorological variables, the meteorological fields will begin to diverge from their true values, i.e., the "model atmosphere." The rms prediction errors displayed in Fig. 1 represent this type of experiment. It would be desirable to use the actual state of the atmosphere and observations taken from the meteorological network to compare the predictive capabilities of various numerical models. Studies by Williamson (1973) and Blumen (1975a, b) suggest that model predictability would be lost much more rapidly than the picture in Fig. 1 suggests. However, "identical twin" experiments have great virtue in Observing Systems Simulation Experiments (OSSE), where answers to questions involving the required accuracy of measurements, density of measurements and frequency of measurements are desired for future planning of the First GARP Global Experiment (FGGE). An excellent overview of these studies has been presented by Kasahara (1972).

Although the typical predictability curves displayed in Fig. 1 are a reflection of nonlinear energy transfer, the treatment of this problem presented by Lorenz does not lend itself to a relatively simple correspondence with predictability experiments generally performed by modeling groups. The present study represents an attempt to provide correspondence between predictability experiments based on analytical solutions of (1) and (2) and experiments with multi-level numerical models. The purpose is to isolate a principal feature of nonlinear transfer that is responsible for the loss of predictability.

The analytical study will proceed as follows: The control state (subscript c) is a solution of (1) given by

$$\Psi_c(x,y,\tau)=\cos(kx+\sigma\tau+ly)+\cos(kx+\sigma\tau-ly)$$
$$=2\cos(kx+\sigma\tau)\cos ly, \tag{7}$$

where Ψ_c denotes the geostrophic streamfunction, (k,l) are (x,y) wavenumbers, and the wave frequency σ is

$$\sigma=\beta k/(k^2+l^2+\lambda^{-2}), \tag{8}$$

while β and λ are defined by (3) and (4). This solution is a westward propagating planetary wave, for which the nonlinear terms in (1) identically vanish. However, suppose we wish to forecast the state of our model atmosphere, without preknowledge of its future state, based on (1) and (2). Then, as shown in A, the appropriate zero-order relationship to balance the initial pressure field $\pi_f(x,y)$, given the initial streamfield $\psi_f(x,y)$, is provided by the geostrophic balance condition. Thus, we set

$$\pi_f(x,y)=\psi_f(x,y). \tag{9}$$

As noted above, a perfect forecast could not be made if observational errors contaminate the initial conditions. Moreover, it is common practice to employ some type of static balance condition, between the mass and wind fields, in the initialization of a primitive equation forecast model. Quite frequently, the so-called balance equation (Charney, 1955), is used as a diagnostic tool to provide the balance between wind and mass fields characteristic of midlatitude flow. However, this balanced state or other initial states of static balance, such as geostrophic balance, may not be accurate representations of the true state of the atmosphere at the initial time. While rationales for using an initial balanced condition have been discussed at length in the literature, ultimately model predictability will be affected if the initial state is not faithfully represented. In the following an example of predictability decay due to an improper initialization procedure, used in conjunction with (1) and (2), will be presented.

We shall assume that the forecast model dynamics are represented by (1) and (2). As noted, the appropriate initial balance between the mass and wind fields is provided by (9). The balance equation, which contains an order Ro correction to geostrophic balance, is given by

$$\Delta\pi_f=\Delta\psi_f+2\,\mathrm{Ro}[(\partial^2\psi_f/\partial x^2)(\partial^2\psi_f/\partial y^2)$$
$$-(\partial^2\psi_f/\partial x\partial y)^2]. \tag{10}$$

In order to examine some consequences of an improper balancing procedure, we shall use (10) rather than (9) for initialization and then compare the forecast with the control state provided by (7).

In order to obtain the solution for the streamfunction $\psi_0(x,y,T,\tau)$, defined in (5), the initial conditions for the

solution of (1) and (2) must be specified. These zero-order initial conditions, derived in A, may be written as

$$\psi_0(x,y)=\Psi(x,y,0)+\psi(x,y,0,0), \tag{11}$$

$$\partial\Delta\psi/\partial T=-\Delta\phi, \tag{12}$$

$$\partial^2\Delta\psi/\partial T^2=-\Delta(\psi_0-\pi), \tag{13}$$

where $\Delta\phi=\partial u/\partial x+\partial v/\partial y$ denotes the Laplacian of the scalar potential of the ageostrophic motion. Condition (12) does not enter into the determination of $\Psi(x,y,\tau)$. We now assume that an initial streamfield from, say, a forecast is available and is given by

$$\psi_f=\hat{a}_1(0)\cos(kx+ly)+\hat{a}_2(0)\cos(kx-ly), \tag{14}$$

where $\hat{a}_1(0)$ and $\hat{a}_2(0)$ denote constant amplitudes. The use of (14) with (10), to balance the initial pressure field, yields

$$\Delta\pi=\Delta\pi_f=\Delta\psi_f+4\,\mathrm{Ro}\,\hat{a}_1(0)\hat{a}_2(0)k^2l^2\times[\cos2ly+\cos2kx]. \tag{15}$$

In general, this pressure field will differ from the true initial field. Moreover, suppose at this time that the true atmospheric state (7),

$$\Psi_c(x,y,0)=\cos(kx+ly)+\cos(kx-ly), \tag{16}$$

is provided by observations. (The situation in which observation errors occur will be discussed in Part II.) The information provided by the observations is used to update the initial streamfield $\psi_0(x,y)$. Consequently, (13) becomes

$$\partial^2\Delta\psi/\partial T^2=-\Delta(\Psi_c-\psi_f)+4\,\mathrm{Ro}\,\hat{a}_1(0)\hat{a}_2(0)k^2l^2\times[\cos2ly+\cos2kx]. \tag{17}$$

As in A, the ageostrophic streamfield $\psi(x,y,T,\tau)$ is determined from (2) and used in (17) to give

$$\psi(x,y,0,0)=a\{[1-\hat{a}_1(0)]\cos(kx+ly)+[1-\hat{a}_2(0)]\cos(kx-ly)\}+\mathrm{Ro}\,\hat{a}_1(0)\hat{a}_2(0)\left\{\frac{k^2}{1+4\lambda^2l^2}\cos2ly+\frac{l^2}{1+4\lambda^2k^2}\cos2kx\right\}, \tag{18}$$

where λ is given by (4), and

$$a=[1+\lambda^2(k^2+l^2)]^{-1}. \tag{19}$$

Note that, even if $\psi_f\equiv\Psi_c$, the improper balancing procedure (10) provides an order Ro contribution to $\partial^2\psi/\partial T^2$ that leads to the generation of gravity-inertia waves. These high-frequency waves may be removed from the solution, after the initial conditions are satisfied, to simulate damping processes characteristic of numerical models (see Williamson and Dickinson, 1972).

Finally, from (11), (16) and (18), the geostrophic initial condition becomes

$$\Psi(x,y,0)=a_1(0)\cos(kx+ly)+a_2(0)\cos(kx-ly)-\mathrm{Ro}\,\hat{a}_1(0)\hat{a}_2(0)\times\left(\frac{k^2}{1+4\lambda^2l^2}\cos2ly+\frac{l^2}{1+4\lambda^2k^2}\cos2kx\right), \tag{20}$$

where

$$\left.\begin{aligned}a_1(0)&=1-a[1-\hat{a}_1(0)]\\ a_2(0)&=1-a[1-\hat{a}_2(0)]\end{aligned}\right\}. \tag{21}$$

Eq. (20) provides the initial condition for the solution of (1)—the forecast.

4. Model predictability

The approximate solution, satisfying (20), is given by

$$\Psi(x,y,\tau)=[a_2(0)\sin\gamma\tau+a_1(0)\cos\gamma\tau]\times\cos(kx+\sigma\tau+ly)+[-a_1(0)\sin\gamma\tau+a_2(0)\cos\gamma\tau]\times\cos(kx+\sigma\tau-ly)-\mathrm{Ro}\,\hat{a}_1(0)\hat{a}_2(0)bk^2\cos2ly, \tag{22}$$

where $a_1(0)$ and $a_2(0)$ are given by (21), and $\hat{a}_1(0)$ and $\hat{a}_2(0)$ by (14); a is defined by (19),

$$b=(1+4\lambda^2l^2)^{-1}, \tag{23}$$

and

$$\gamma=\mathrm{Ro}\,\hat{a}_1(0)\hat{a}_2(0)ab\lambda^2lk^3(k^2-3l^2). \tag{24}$$

The development leading to (22) appears in the Appendix.

The true atmospheric state, given by (7), represents a planetary wave moving at constant phase speed σ/k. The forecast solutions determined from a perfect model but imperfect initial condition, is a stationary zonal current, that neither gains nor loses energy, but acts as a catalyst enabling energy to be exchanged between the two waves that both propagate at speed σ/k.

The normalized rms forecast error is defined as

$$r(\tau)=\{\overline{|\Psi_c-\Psi|^2}/\overline{|\Psi_c|^2}\}^{\frac{1}{2}}, \tag{25}$$

where the bar denotes the average over one wavelength. Evaluation of (25) with (7) and (22) yields

$$r(\tau)=\tfrac{1}{2}\{[1-a_1(\tau)]^2+[1-a_2(\tau)]^2+a_3^2\}^{\frac{1}{2}}, \tag{26}$$

where $a_1(\tau)$, $a_2(\tau)$ and a_3 denote the amplitudes of the three waves in (22), given by

$$\left.\begin{aligned}a_1(\tau)&=a_2(0)\sin\gamma\tau+a_1(0)\cos\gamma\tau\\ a_2(\tau)&=-a_1(0)\sin\gamma\tau+a_2(0)\cos\gamma\tau\\ a_3&=-\mathrm{Ro}\,\hat{a}_1(0)\hat{a}_2(0)bk^2\end{aligned}\right\}. \tag{27}$$

Error growth, represented by $r(\tau)$, will be examined for three cases:

1) $\hat{a}_1(0)=1+\epsilon$, $\hat{a}_2(0)=1$.

2) $\hat{a}_1(0)=\hat{a}_2(0)=1+\epsilon$.

3) $\hat{a}_1(0)=\hat{a}_2(0)=1$.

The parameter ϵ denotes a random error in the initial streamfield, given by (14). Error growth in cases 1) and 2) is associated only with improper initialization. Case 3) will be considered in Section 5, in association with differences in phase speed between the forecast and control solutions.

The following characteristic values, typical of midlatitude flow, are used for normalization:

$$\left.\begin{array}{l} L=L_x/4=L_y/4=(\pi/2)\times 10^6 \text{ m}, \quad k=2\pi L/L_x=\pi/2 \\ l=2\pi L/L_y=\pi/2, \quad g'=0.625 \text{ m s}^{-1}, \quad D_0=8\times 10^3 \text{ m} \\ f_0=10^{-4} \text{ s}^{-1} \end{array}\right\}.$$

These values yield

$$\lambda^2(k^2+l^2)=1, \quad a=0.5, \quad b=0.333.$$

We choose $\tau=1$ to correspond to one day and $\text{Ro}=10^{-1}$.

The random initial error ϵ is assumed to have a rectangular probability distribution,

$$\left.\begin{array}{ll} p(\epsilon)=1/2\alpha, & |\epsilon|\leqslant\alpha \\ p(\epsilon)=0, & |\epsilon|>\alpha \end{array}\right\}. \tag{28}$$

This type of distribution was used by Williamson and Kasahara (1971) in their predictability and updating experiments. The expected value of the rms forecast error is determined from (26), (27) and (28). For case 1),

$$(\langle r^2(\tau)\rangle)^{\frac{1}{2}}=\left\{2\left[1-\cos z\frac{\sin\alpha z}{\alpha z}\right]-\frac{a}{z}(\cos z-\sin z)\left(\frac{\sin\alpha z}{\alpha z}-\cos\alpha z\right)+\tfrac{1}{2}[(a\alpha)^2/3+(\text{Ro } bk^2)^2(1+\alpha^2/3)]\right\}^{\frac{1}{2}}, \tag{29}$$

where the angle brackets denote a statistical average, and

$$z=\text{Ro } ab\lambda^2lk^3(3l^2-k^2)\tau = 10^{-1}\tau, \tag{30}$$

using the characteristic parameter values listed above. For case 2),

$$(\langle r^2(\tau)\rangle)^{\frac{1}{2}}=\left\{2\left[1-\frac{(1-a)}{2\alpha}\left(\frac{\pi}{2z}\right)^{\frac{1}{2}}\times(C(X_1)-C(X_2))\right]-2a\cos(1+\alpha^2)z\frac{\sin 2\alpha z}{2\alpha z}+(a\alpha)^2/3+\tfrac{1}{2}(\text{Ro } bk^2)^2(1+2\alpha^2+\alpha^4/5)\right\}^{\frac{1}{2}}, \tag{31}$$

where z is given by (30),

$$\left.\begin{array}{l} X_1=(2z/\pi)^{\frac{1}{2}}(1+\alpha) \\ X_2=(2z/\pi)^{\frac{1}{2}}(1-\alpha) \end{array}\right\}, \tag{32}$$

and $C(X_1)$ and $C(X_2)$ are Fresnel integrals (Abramowitz and Stegun, 1964, Section 7.3) defined by

$$C(X)\equiv\int_0^X\cos\left(\frac{\pi}{2}t^2\right)dt. \tag{33}$$

The expression for $r(\tau)$, corresponding to case 3), may be determined by setting $\alpha=0$ in (29). We obtain

$$(\langle r^2(\tau)\rangle)^{\frac{1}{2}}=r(\tau)=\{2[1-\cos z]+\tfrac{1}{2}(\text{Ro } bk^2)^2\}^{\frac{1}{2}}. \tag{34}$$

The expected values of the rms errors corresponding to the first two cases presented above are shown in Figs. 2 and 3. The asymptote in Figs. 2 and 3 is effectively $2^{\frac{1}{2}}$ because the contribution from the last two terms in (29) and (31) is order 2% or less. A comparison of Figs. 2 and 3 with Fig. 1 shows that the present model captures the basic features of error growth characteristic of numerical models. In particular, the initial error decrease shown in Fig. 1 is also reproduced in Fig. 2, but the presence of this initial adjustment in the present model depends upon initial conditions; it does not appear in case 2). The characteristic doubling time for initial errors ranges from 1 day ($\alpha=0.1$) to about 3.5 days ($\alpha=1.0$). These times are somewhat shorter than the doubling time of about 2–6 days found by Williamson and Kasahara (1971). Results from the NCAR GCM and other models show that the asymptotic error level is reached in about 4–5 weeks. This is also a characteristic time for a broad range of initial errors in this model, but the time is reduced for large initial errors in case 2). The damping of the error growth curve is enhanced by increasing the maximum range of the initial error in the probability distribution (28). This added uncertainty in the initial state is reflected in the nonlinear growth rate γ. Consequently, the expected value of the rms forecast error [(29) or (31)] shows a reduction in amplitude as the asymptote is approached that reflects the effect of averaging the error growth over all possible initial states. This latter feature does not appear in case 3), because the rms forecast error represents an undamped oscillation about the asymptote. However, it is particularly noteworthy that the asymptotic error level, in Figs. 2 and 3, is essentially independent of the initial error, a result deduced by Lorenz and suggested by numerical experimentation.

The present results are typical for scales of motion characteristic of quasi-geostrophic midlatitude flow. Since the model was developed from the requirement that $\text{Ro}\ll 1$, the growth rate γ of the amplitude modulation is of order Ro for these scales of motion. Before

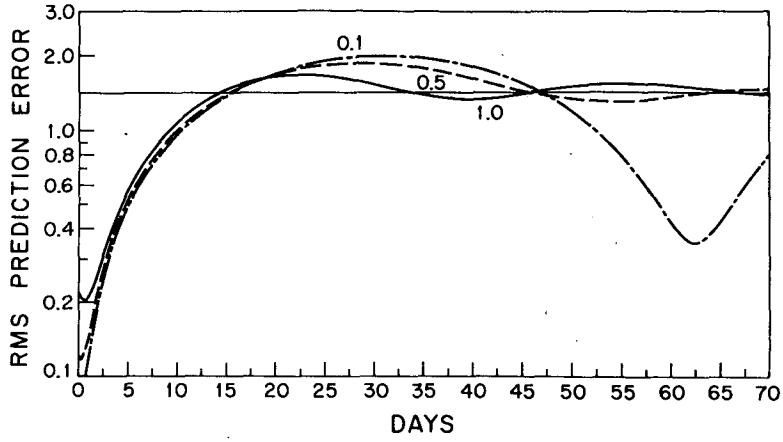

FIG. 2. Growth of rms prediction error for case 1), given by Eq. (29). The three curves correspond to the maximum amplitude error bounds $|\alpha|=0.1$, 0.5 and 1.0. The parameter values are given in the text.

offering an interpretation of these results, an analogous problem of predictability, when phase errors exist between the model solutions and the true atmospheric state, will be examined.

5. Phase errors

The rms prediction error, corresponding to differences in phase speed between the wave solution of the model (1) and the assumed control state, was examined in A. Only the error corresponding to linear solutions of (1) was examined. Now this error will be computed for the case when the control state is still represented by (7), but (7) is *not* a solution of the model equation used for producing a forecast solution. For present purposes, the model deficiency is simply introduced by defining λ_c, given by (4), as the control value and $\lambda \neq \lambda_c$ as the radius of deformation for the model. Correspondingly, the control wave (7) is characterized by a phase speed σ_c/k, while the phase speed of the planetary wave solution of the imperfect model (22) is $\sigma/k \neq \sigma_c/k$, where (σ,σ_c) are given by (8) with the appropriate value of the radius of deformation λ used.

For simplicity, only the case 3) will be considered: at $\tau=0$, the correct streamfield given by (7) is used for initialization with the balance equation (10). For this case, $\hat{a}_1(0)=\hat{a}_2(0)=1$ in (14). Then (7) and (22) yield

$$\Psi_c-\Psi=\cos(kx+\sigma_c\tau+ly)-a_1(\tau)\cos(kx+\sigma\tau+ly)+\cos(kx+\sigma_c\tau-ly)-a_2(\tau)\cos(kx+\sigma\tau-ly)+\mathrm{Ro}\,bk^2\cos 2ly, \quad (35)$$

where a_1 and a_2 are given by (27) corresponding to case 3). If (35) is substituted into (25), the rms forecast error for this case becomes

$$r(\tau)=\{2[1-\cos\gamma\tau\cos(\sigma_c-\sigma)\tau]+\tfrac{1}{2}(\mathrm{Ro}\,bk^2)^2\}^{\frac{1}{2}}, \quad (36)$$

where γ, given by (24), is

$$\gamma=\mathrm{Ro}\,ab\lambda^2lk^3(k^2-3l^2). \quad (37)$$

The expression for the error corresponding to a *linear* forecast solution is

$$r(\tau)=\{2[1-\cos(\sigma_c-\sigma)\tau]\}^{\frac{1}{2}} \quad (38)$$

found by setting Ro=0 in (36). The nonlinearity, in

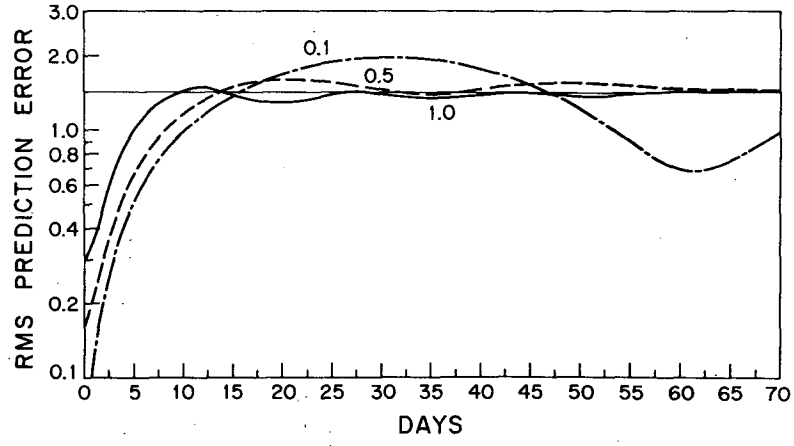

FIG. 3. As in Fig. 2 except case 2), given by Eq. (31).

this case, introduces an amplitude modulation and a constant error from the presence of the zonal flow in (35).

Suppose $\sigma_c - \sigma$ is a random variable with zero mean having the rectangular probability distribution given by (28). The expected value of the rms prediction error is

$$(\langle \tau^2(\tau) \rangle)^{\frac{1}{2}} = \left\{ 2\left[1 - \cos\gamma\tau \frac{\sin\alpha\tau}{\alpha\tau} \right] + \tfrac{1}{2}(\mathrm{Ro}\, bk^2)^2 \right\}^{\frac{1}{2}}, \quad (39)$$

where α should now be interpreted as the maximum phase error. For the parameter values used in Section 4, $|\alpha| = 0.1$ corresponds to a phase propagation error of 55 km day^{-1}. The predictability error growth is shown in Fig. 4 for various values of α and $|\gamma| = 0.1$, the value used in (29). The significant result of the present computation is that predictability error growth due to random phase errors between the model solutions and the control state is very similar to the error growth arising from initial amplitude errors. However, a comparison of Figs. 2 and 4, for example, shows that the presence of random phase errors provides more stringent amplitude modulation of the error oscillations, for $|\alpha| \gtrsim 0.1$, than that provided by the initial amplitude errors. Moreover, the present results may explain the growth rate associated with curve 4 in Fig. 1. This curve represents the rms error from changing the model physics slightly from that of the control state, but not introducing an initial amplitude error. This was accomplished by increasing a turbulent exchange coefficient by one order of magnitude. The intent of this experiment was to demonstrate that "the predictability of the real atmosphere is also limited by uncertainty in our knowledge of parameterization of physics incorporated in the prediction models." The present experiment, however, cannot be interpreted strictly as an assessment of the role of a physical parameterization on atmospheric predictability: error energy in the present model is only exchanged between two wave components rather than by transfer through a broad spectral range. Nonetheless, the present case does appear to represent a simple analogue of the model change made by Williamson and Kasahara because all the model physics in (1) is incorporated in the radius of deformation λ. As a consequence, it is suggested that the error growth depicted by curve 4 in Fig. 1 is due to phase errors. If this interpretation is correct, correspondence with the present results would suggest that $|\alpha| \lesssim 0.1$.

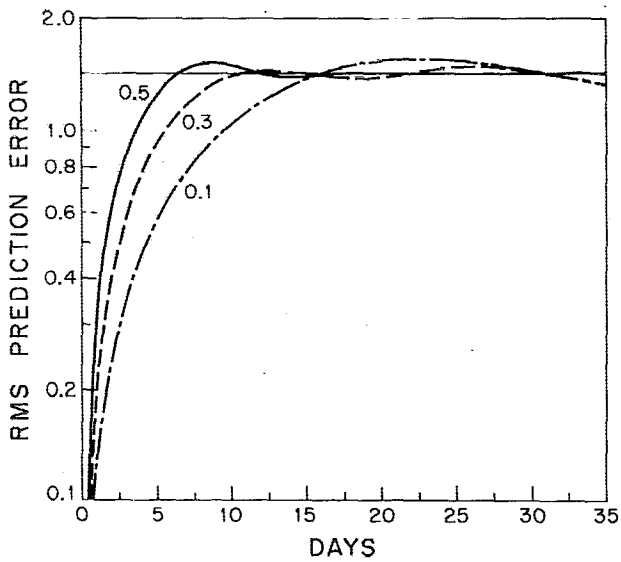

FIG. 4. As in Fig. 2 except case 3), given by Eq. (39). The curves correspond to maximum phase errors $|\alpha| = 0.1$, 0.3 and 0.5.

6. Remarks

A relatively simple divergent barotropic model has been used to study atmospheric predictability. This study was concerned with nonlinear error growth, relative to a model-determined control state, produced by an initialization procedure that is *not* compatible with the model equations. The intent was to provide insight into the mechanism of predictability decay produced by more complex primitive equation models which utilize initialization schemes that, to some extent, are not compatible with the model dynamics. Any improper method of initialization will ultimately lead to loss of predictability. The time-scale for this decay will depend on the particular model chosen for study. Here we are concerned with the characteristic growth associated with large-scale numerical models that exhibit forecast-error doubling-times of the order of a few days.

In the present study, the balance equation (10) was used for initialization as an example of an improper initialization procedure: geostrophic balance is actually the initial balance condition that is consistent with the development of the model equations (1) and (2). Subsequent error growth by nonlinear energy exchange occurs because the initial field is altered, as is evident by comparing (20) with the control state (7).

The question arises whether the present results are indicative of nonlinear processes that lead to loss of predictability in primitive equation models. Objections that may be raised include: (i) the possibility of different results if an initialization scheme other than the balance equation had been used; (ii) the fact that in primitive equation models quasi-geostrophic and ageostrophic modes do not evolve independently but may interact to provide additional complexity to the dynamics of predictability decay; and (iii) the use of a rather special triad solution to demonstrate nonlinear processes that occur in models with many more allowable degrees of freedom. These objections, as well as others that might be raised, cannot be dismissed. However, comparison of the present model results with numerical experiments suggests that the present model dynamics has captured some of the essence of the

dynamics of the more complicated primitive equation models.

In particular, error growth in the present model compared very well with experiments carried out with the NCAR GCM, which are typical of numerical experiments performed with other models (e.g., see Kasahara, 1972). The comparison is made between the GCM results presented in Fig. 1 and the model results in Figs. 2–4. Moreover, the present results show that the characteristic error growth leading to predictability decay occurs by relatively slow, periodic, nonlinear energy exchange between two planetary waves; the existence of a stationary zonal flow, that forms the third mode of the triad solutions of the forecast equation, only adds a negligibly small increase to the asymptotic error level. *In effect, the characteristic error growth curves, produced by numerical models, can be simulated by nonlinear energy exchange between relatively few waves, occurring on a long time-scale compared to the characteristic period of planetary waves.*

The present results are not dependent on the specific use of the balance equation as an initialization scheme. The balance equation provided a convenient mechanism to alter the initial field to the extent that a triad solution could be generated. Other initializations could be incorporated to accomplish the same purpose. However, the important point here is not which initialization scheme has been employed, but that the characteristic loss of predictability may be modeled by a relatively small number of nonlinear interactions. In practice, slow nonlinear energy exchange between long planetary waves forced by orography and continentality may, in fact, make a significant contribution to the error growth characteristic of GCM predictability experiments. The importance of this latter process is suggested by the fact that this low wavenumber part of the wave spectrum generally contains a significant portion of the total atmospheric energy. Moreover, error growth is essentially independent of the initialization procedure used in these numerical studies.

Alternatively, NCAR GCM predictability experiments do show that the spectrum of error kinetic energy for high wavenumbers evolves in a manner similar to Leith's (1971) deductions based on a model of two-dimensional turbulence using Cartesian geometry; the longer waves appear to be outside the cascading inertial range of this theory. As noted in Section 3, some other deductions based on a model of two-dimensional turbulence are in accord with the results obtained with large-scale numerical models as well as with the results obtained in the present study. The present model conserves energy and potential enstrophy, as in a model of two-dimensional turbulence, but the typical predictability decay that is simulated here is not a cascade process. Thus the present study raises questions concerning the relative importance of various mechanisms, that lead to loss of predictability by atmospheric models, which include barotropic and baroclinic instability mechanisms in addition to those noted above.

Finally, the contribution to error growth from interactions between quasi-geostrophic and ageostrophic modes has not been definitively established. However, predictability experiments performed by Williamson and Kasahara (1971, Section 6) show that the geostrophic adjustment process, as described by *linear* theory, is verified in some cases, although completely satisfactory agreement is not attained. Another consideration is the fact that, on a global basis, the ratio of ageostrophic to geostrophic energy is relatively small. Consequently, the tentative conclusion is that present evidence does not indicate that interactions between geostrophic and ageostrophic modes is a significant feature of predictability decay in midlatitude flow, although some contribution to loss of predictability could be expected.

The present study does not appear to offer an obvious solution or even a firm promise that forecast error growth can be controlled in the near future. However, the isolation of what appears to be a fundamental process producing error growth in numerical models should be kept in view when model changes are planned. In particular, the present results suggest that implementation of model changes that better represent topographic forcing and the radiative processes that control the distribution of large-scale heat sources and sinks could lead to forecast improvement, at least of the long-wave part of the atmospheric energy spectrum. Although it would be necessary to dissipate energy, provided by such forcing, the results obtained here also appear to suggest that short- and, perhaps, medium-range predictions of long waves should not be particularly sensitive to parameterizations of subgrid-scale processes. However, additional evidence from experimentation with numerical models would be required to either support or refute the conjectures that have been drawn from the present study.

Acknowledgments. I wish to thank Akira Kasahara and David Williamson for permission to use Fig. 1 in the text, and Perry Witt for computational help. This investigation was supported by the Atmospheric Science Section of the National Science Foundation, under Grant GA-31868.

APPENDIX

Nonlinear Triad Solution

An approximate solution of (1), satisfying the initial condition (20), has been presented by Longuet-Higgins and Gill (1967). First a solution is found that satisfies (20) with the $\cos 2kx$ term neglected. The solution, given by (22), forms a resonant triplet satisfying the necessary conditions

$$\left.\begin{aligned} k_1+k_2+k_3&=0\\ l_1+l_2+l_3&=0\\ \sigma_1+\sigma_2+\sigma_3&=0 \end{aligned}\right\}, \tag{A1}$$

where $k=k_1=-k_2$, $k_3=0$; $l=l_1=l_2$, $l_3=-2l$; $\sigma=\sigma_1=-\sigma_2$, $\sigma_3=0$; and each wave satisfies the dispersion relation

$$\sigma(k^2+l^2+\lambda^{-2})-\beta k=0. \tag{A2}$$

The amplitudes $a_i(\tau)$, $i=1,2,3$, satisfy

$$\left.\begin{aligned}\dot{a}_1&=-a_2a_3(k^2-3l^2)l\sigma/\beta\\ \dot{a}_2&=a_1a_3(k^2-3l^2)l\sigma/\beta\\ \dot{a}_3&=0\end{aligned}\right\}, \tag{A3}$$

where the dot denotes time differentiation. The general solutions of (A3) are

$$\left.\begin{aligned}a_1&=A_1\cos\gamma\tau+B_1\sin\gamma\tau\\ a_2&=A_2\cos\gamma\tau+B_2\sin\gamma\tau\\ a_3&=A_3\end{aligned}\right\}, \tag{A4}$$

where γ is given by (24) and the A_i and B_i are constants evaluated from the initial condition (20). Note that when $k^2-3l^2=0$, the a_i are constants and the nonlinear terms in (1) sum to zero.

The terms neglected in the derivation of (22) correspond to forced waves which do not give rise to resonant energy exchange, as described by (A3), i.e., the forced wave solutions do not satisfy (A2). The necessary conditions to justify neglecting the forced waves are shown, by Longuet-Higgins and Gill, to be $\mathrm{Ro}\ll 1$, a condition already imposed on the present model. Alternatively, within the present context, (22) may be taken as a forecast solution, satisfying a model of atmospheric flow, which is derived by smoothing the meteorological fields, for example, in order to retain only the three terms appearing in (22). Finally, it is noted that both energy and potential enstrophy (one-half the mean squared potential vorticity) are conserved in the present model.

REFERENCES

Abramowitz, M., and I. A. Stegun, 1964: *Handbook of Mathematical Functions*. Washington, D. C., Govt. Printing Office, 1046 pp.

Bengtsson, L., 1975: Four-dimensional assimilation of meteorological observations. GARP Publ. Ser., No. 15, WMO-ICSU Joint Organizing Committee, 76 pp.

Blumen, W., 1972: Geostrophic adjustment. *Rev. Geophys. Space Phys.*, **10**, 485–528.

——, 1975a: An analytical view of updating meteorological variables: Part I. Phase errors. *J. Atmos. Sci.*, **32**. 274–286.

——, 1975b: An analytical view of updating meteorological variables: Part II. Weighted assimilation. *J. Atmos. Sci.*, **32**, 690–697.

Charney, J. G., 1955: The use of the primitive equations of motion in numerical weather prediction. *Tellus*, **7**, 22–26.

Kasahara, A., 1972: Simulation experiments for meteorological observing systems for GARP. *Bull. Amer. Meteor. Soc.*, **53**, 252–264.

Leith, C. E., 1971: Atmospheric predictability and two-dimensional turbulence. *J. Atmos. Sci.*, **28**, 145–161.

Longuet-Higgins, M. S., and A. E. Gill, 1967: Resonant interactions between planetary waves. *Proc. Roy. Soc. London*, **A299**, 120–140.

Lorenz, E. N., 1969: The predictability of a flow which possesses many scales of motion. *Tellus*, **21**, 289–307.

Williamson, D., 1973: The effect of forecast error accumulation on four-dimensional data assimilation. *J. Atmos. Sci.*, **30**, 537–543.

——, and R. Dickinson, 1972: Periodic updating of meteorological variables. *J. Atmos. Sci.*, **19**, 190–193.

——, and A. Kasahara, 1971: Adaptation of meteorological variables forced by updating. *J. Atmos. Sci.*, **28**, 1313–1324.